

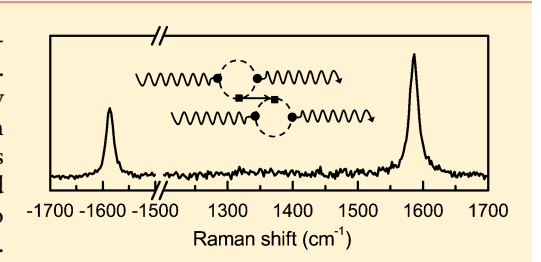


pubs.acs.org/NanoLett

# Optical-Phonon Resonances with Saddle-Point Excitons in Twisted-Bilayer Graphene

Ado Jorio,\*\*,†,‡ Mark Kasperczyk,† Nick Clark,¶ Elke Neu,§ Patrick Maletinsky,§ Aravind Vijayaraghavan,¶ and Lukas Novotny

ABSTRACT: Twisted-bilayer graphene (tBLG) exhibits van Hove singularities in the density of states that can be tuned by changing the twisting angle  $\theta$ . A  $\theta$ -defined tBLG has been produced and characterized with optical reflectivity and resonance Raman scattering. The  $\theta$ -engineered optical response is shown to be consistent with persistent saddle-point excitons. Separate resonances with Stokes and anti-Stokes Raman scattering components can be achieved due to the sharpness of the two-dimensional saddle-point excitons, similar to what has been previously observed for one-dimensional carbon nanotubes. The excitation power dependence for the Stokes and anti-Stokes emissions



indicate that the two processes are correlated and that they share the same phonon.

KEYWORDS: Graphene, Raman scattering, optical reflectivity, coherence

C addle points in the electron dispersion of two-dimensional systems generate logarithmically diverging van-Hove singularities (vHs) in the density of states (DOS). In singlelayer graphene (Figure 1a), the vHs occur at the M point for both the valence  $(\pi)$  and conduction  $(\pi^*)$  bands (Figure 1b) and consequently in the joint density of sates (JDOS) for optical properties. The JDOS vHs falls into the ultraviolet frequency region in graphene,<sup>2</sup> as well as the related peak in the optical conductivity  $(E_{\rm opt})$ , which should be redshifted from the JDOS vHs due to excitonic effects.3

Twisted-bilayer graphene (tBLG) is formed by adding a twist angle  $\theta$  between two graphene layers on top of each other.<sup>4-7</sup> The expansion of the real lattice parameter when building a superstructured tBLG (see arrow in Figure 1c) generates a shrinking of the reciprocal space (Figure 1d), thus bringing the Dirac (K and K') points close together and moving them closer to the M saddle point. Consequently, the vHs will shift in energy, thereby redshifting the JDOS vHs to visible frequencies and even into the far-infrared, depending on the twisting angle  $\theta$ . This effect has been measured in tBLG using scanning tunneling spectroscopy<sup>6</sup> and it has been explored using Raman spectroscopy.<sup>7–16</sup>

Until now, the studied tBLGs have been produced randomly, that is, without controlling the twist angle  $\theta$ . Furthermore, the generated 2D vHs have been directly measured only by scanning tunneling spectroscopy,<sup>6</sup> which is limited to energies near the Fermi level and is usually more invasive and less accurate than optical measurements. Here we report the production and optical characterization of a tBLG with a previously selected  $\theta$  angle, chosen specifically to explore Stokes and anti-Stokes resonance Raman scattering effects. By mode-engineering the system to work in resonance with the anti-Stokes line, we observe a quadratic power dependence of the anti-Stokes process. This power dependence is indicative of Stokes-induced anti-Stokes scattering in which the phonon generated by the Stokes scattering is consumed by the anti-Stokes process.

Resonance Raman studies show that the peak in the optical conductivity is given by  $E_{\rm opt} = E_0 \sin(3\theta)$  with  $E_0 = 3.9$  eV obtained experimentally. By choosing  $\theta = 11.3^{\circ}$ , we expect  $E_{\rm opt}$  = 2.175 eV. Our tBLG sample was prepared as follows: two mechanically exfoliated single-layer graphene flakes with welldefined edges were found on top of a solid SiO2 surface. The samples are shown in the optical images in Figure 2a,b, where the well-defined edge directions are indicated by the larger and smaller white lines, respectively, as sufficient indication of either zigzag or armchair crystallographic orientations. In sequence, one of the graphene flakes was transferred and placed on top of the second flake with the well-defined edge rotated with respect to the second by an angle  $\theta = 11 \pm 1^{\circ}$ , as indicated by translation of the larger white line from Figure 2a into Figure 2b. Then the  $\theta$  = 11  $\pm$  1° tBLG was transferred onto a 500 nm thick SiN, membrane perforated with holes of 10  $\mu$ m diameter (see optical image in Figure 2c and schematics in Figure 2d). Because the samples have areas with bi-, tri-, and many-layer graphene, it is only where the monolayers of each flake overlap

Received: June 27, 2014 Revised: August 18, 2014 Published: September 8, 2014



<sup>†</sup>Photonics Laboratory, ETH Zürich, 8093 Zürich, Switzerland

<sup>&</sup>lt;sup>‡</sup>Departamento de Física, Universidade Federal de Minas Gerais, Belo Horizonte, MG 31270-901, Brazil

<sup>&</sup>lt;sup>¶</sup>School of Materials and National Graphene Institute, The University of Manchester, Manchester M13 9PL United Kingdom

<sup>§</sup>Department of Physics, University of Basel, Klingelbergstrasse 82, CH-4056 Basel, Switzerland

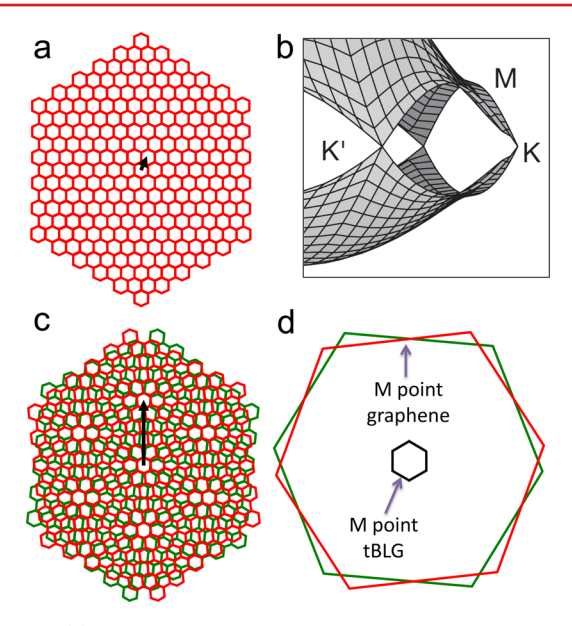


**Figure 1.** (a) Illustration of a single-layer graphene in real space, and (b) the dispersion of the  $\pi$  and  $\pi^*$  electrons at the edge of the Brillouin zone, close to the Dirac (K and K') and saddle (M) points. (c) Illustration of a tBLG showing the superstructure Moiré pattern that defines the increased lattice periodicity (arrow). (d) The first Brillouin zones of the two single-layer graphenes (green and red) and of the tBLG (black). The location of the M points are indicated.

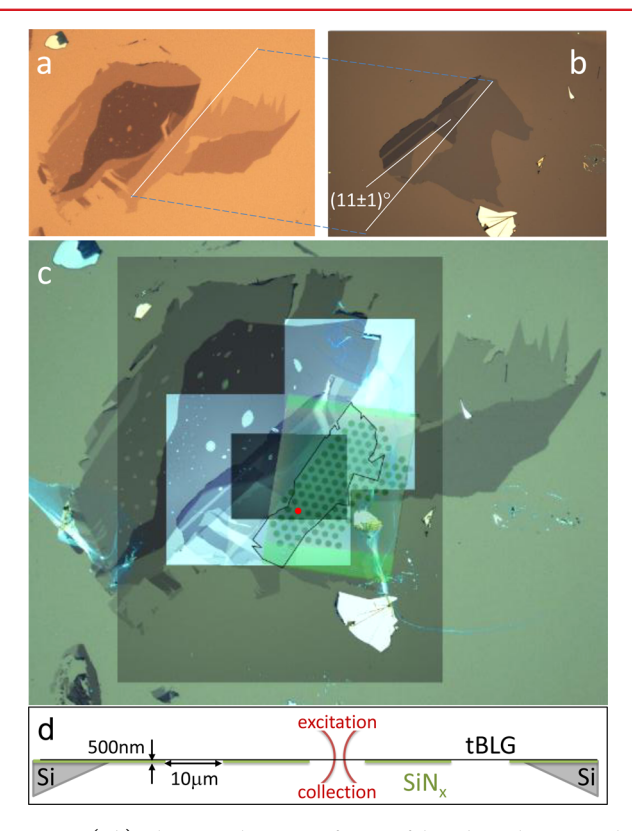
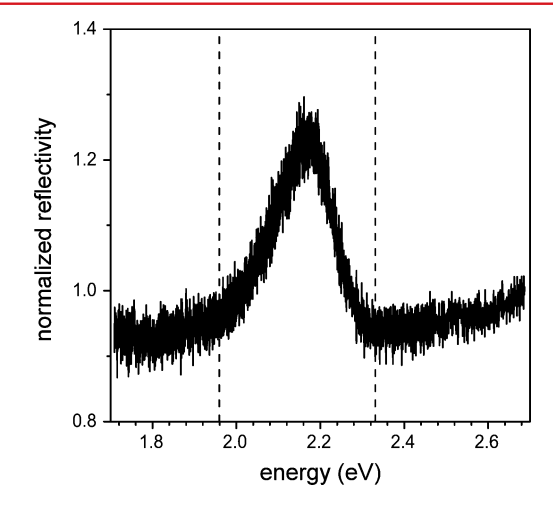


Figure 2. (a,b) The optical images of two exfoliated graphene samples with well-defined edges (see white traces). The two graphene samples were superimposed with an angle  $\theta=(11\pm1)^\circ$  between the well-defined edges. The twisted bilayer graphene (tBLG) is then deposited on top of a Si substrate with a 500 nm thick layer of SiN<sub>x</sub>, perforated with 10  $\mu$ m diameter holes (optical image in (c) and schematics in (d)). The red dot in (c) indicates the hole where the specific tBLG experiments reported here were performed.

that the tBLG is present. In the image in Figure 2c, a dark contour outlines where the tBLG occurs. Notice that while well-defined edges are a sufficient indication of crystallographic orientation, armchair or zigzag cannot be differentiated optically, and the procedure here has 50% chance of generating a  $(30^{\circ} + \theta)$  angle, rather than the wanted  $\theta$ . A reference sample with  $\theta = 0^{\circ}$  was also fabricated by directly depositing a mechanically exfoliated AB-stacked bilayer graphene (AB-BLG) onto a similar 500 nm thick SiN $_x$  membrane perforated with holes of 10  $\mu$ m diameter (not shown). All experiments were performed in the freely suspended regions of the graphene tBLG and AB-BLG, that is, in the holes of the SiN $_x$  membranes. This excludes any substrate-related background scattering and artifacts.

Figure 3 shows the reflectivity of the tBLG shown in Figure 2c, measured with a supercontinuum laser and normalized to



**Figure 3.** Reflectivity of the tBLG normalized by the reflectivity of AB-BLG. The vertical dashed lines show the energies of the excitation lasers  $E_{\rm laser} = 1.96$  eV and  $E_{\rm laser} = 2.33$  eV.

the response of the AB-BLG. The tBLG reflectivity peak is observed at  $E_{\rm opt}=2.18$  eV, in excellent agreement with the prediction for  $\theta=11.3^{\circ}.^{16}$  The asymmetric reflectivity line shape observed in the ultraviolet for graphene has been identified as a result of the convolution between a well-defined (excitonic) transition with a continuum density of electronic states, which results in a Fano resonance feature. The asymmetric line shape shown in Figure 3 is fully consistent with this picture, showing that many-body effects leading to the formation of two-dimensional saddle-point excitons are persistent, remaining in the modified structure of tBLG, as discussed by Havener et al. The excellent agreement with the production of two-dimensional saddle-point excitons are persistent, remaining in the modified structure of tBLG, as discussed by Havener et al.

Having properly characterized the energy of the saddle-point exciton ( $E_{\rm opt}=2.18~{\rm eV}$ ), we can now explore different phenomena in the resonance Raman scattering. Figure 4 shows the anti-Stokes and Stokes G band Raman spectra for AB-BLG (a,b) and tBLG (c,d). In Figure 4a,c, the samples were excited with a frequency doubled YAG laser at  $E_{\rm laser}=2.33~{\rm eV}$  ( $\lambda_{\rm laser}=532.0~{\rm nm}$ ), while in Figure 4b,d the samples were excited with a HeNe laser at  $E_{\rm laser}=1.96~{\rm eV}$  ( $\lambda_{\rm laser}=632.8~{\rm nm}$ ). These two laser energies are marked in Figure 3 by the vertical dashed lines. Notice that the two lasers are off resonance with respect to the saddle-point exciton,  $E_{\rm laser}$  being blue- or red-shifted from  $E_{\rm opt}$  by approximately the G band phonon energy ( $E_{\rm G}=0.2~{\rm eV}$ ).

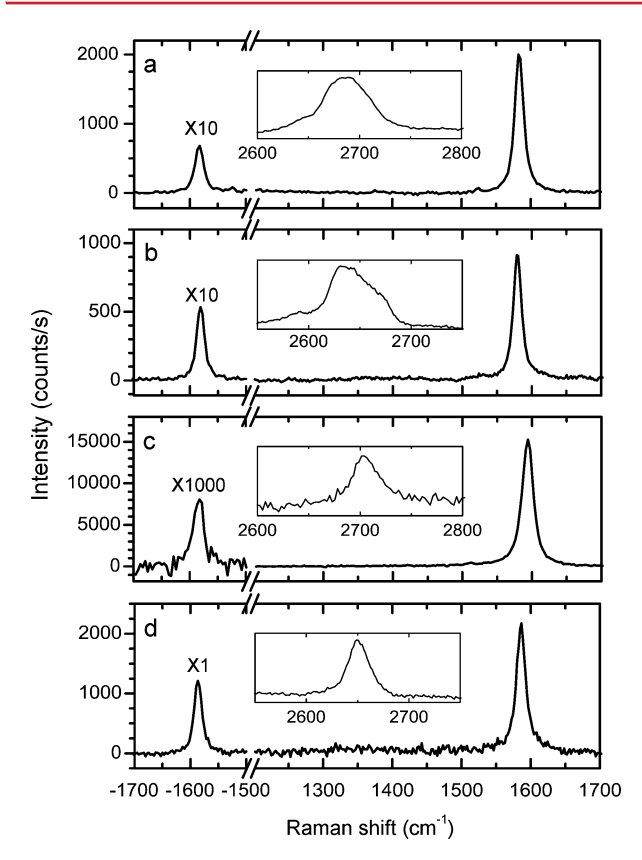
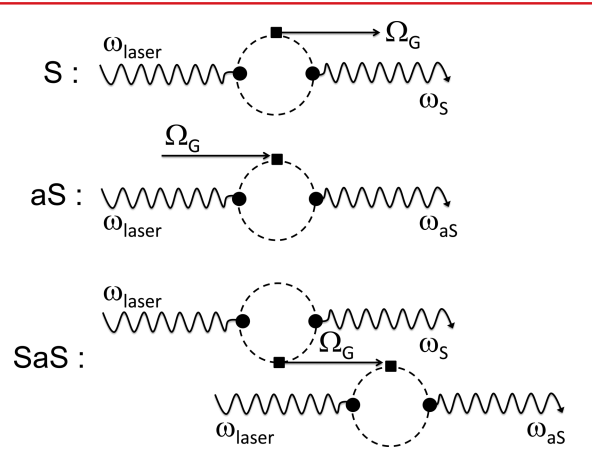


Figure 4. Stokes and anti-Stokes Raman spectra of AB-BLG (a,b) and tBLG (c,d). Panels a and c have been obtained with excitation at  $E_{laser}$ = 2.33 eV, while panels b and d have been obtained with excitation at  $E_{\rm laser}$  = 1.96 eV. All spectra have been acquired with  $P_{\rm laser} \sim 5$  mW reaching the sample through an air objective (NA = 0.8). The signal is collected in transmission by another air objective with larger NA (= 0.9). The Stokes spectra are displayed down to 1200 cm<sup>-1</sup> to highlight the absence of the disorder-induced (D) band. The insets show the respective second-order G' (or 2D) bands, characteristic for ABstacked (a,b) and misoriented (c,d) bilayer graphene. The anti-Stokes signals are magnified for clarity (magnification indicated on top of the respective peaks). All spectra have been corrected to account for detector (charged-coupled device from Excelon - Pixis 100B) and spectrometer (Acton SP2300 from Princeton Instruments, equipped with a 600 grooves/mm grating blazed at 750 nm) nominal efficiencies.

In the AB-BLG case (Figure 4a,b), the Stokes and anti-Stokes signals do not change significantly when changing the excitation laser energy. The spectra obtained with  $E_{\text{laser}} = 2.33 \text{ eV}$  is only two times more intense than the spectra obtained with  $E_{\text{laser}}$  = 1.96 eV (see Figure 4a,b, respectively), due to the  $E_{\text{laser}}^4$ dependence of the G-band scattering cross section.<sup>2,18</sup> The intensity ratio between the Stokes and the anti-Stokes peaks  $(I_{aS}/I_S)$  is basically unchanged. However, in the case of tBLG, the spectra change significantly when changing the excitation laser energy. Figure 4c ( $E_{laser} = 2.33 \text{ eV}$ ) shows a Stokes signal ~10 times stronger than the signal obtained from the AB-BLG, while the anti-Stokes signal is ~10 times weaker. On the other hand, Figure 4d ( $E_{laser} = 1.96 \text{ eV}$ ) shows a Stokes signal with comparable intensity but an anti-Stokes signal ~10 times stronger than in the AB-BLG. The  $I_{aS}/I_{S}$  ratio thus changes by 3 orders of magnitude when comparing the measurements with  $E_{\rm laser} = 2.33 \, {\rm eV}$  and  $E_{\rm laser} = 1.96 \, {\rm eV}$ . This result happens because, while the  $E_{\text{laser}} = 1.96$  eV laser leads to a resonance with the anti-Stokes photon emission, the  $E_{laser} = 2.33$  eV laser gives rise to a resonance with the Stokes photon emission. Qualitatively, similar Stokes versus anti-Stokes resonances were observed in one-dimensional (1D) carbon nanotubes, <sup>19</sup> where sharp resonances are characteristics of the 1D band structure. <sup>20</sup> Interestingly, similar effects can be observed in a two-dimensional graphene system due to the saddle-point exciton resonance.

Notice that in Figure 4d, the anti-Stokes G band signal intensity is close to the Stokes intensity. Although similar anti-Stokes scattering resonance has been observed in carbon nanotubes before, <sup>19,20</sup> an important question remains: where do these high energy G band phonons, which are being annihilated in the highly efficient resonant anti-Stokes emission, come from? To answer this question, we refer to the Feynman diagrams shown in Figure 5. The S diagram shows the Stokes



**Figure 5.** Feynman diagrams for three different Raman scattering processes. Wavy and straight arrows stand for photons and phonons, respectively, while the dashed circles represent electron—hole pairs. Black dots and black squares represent electron—photon and electron—phonon interactions. S stands for Stokes Raman process, aS for anti-Stokes Raman process, and the last diagram, named here SaS, represents the generation of a Stokes and anti-Stokes photon pair via creation and annihilation of the same phonon.

Raman scattering event where a phonon and a Stokes-shifted Raman photon are generated. The aS diagram shows the anti-Stokes Raman scattering process, where one existing phonon is annihilated, generating the anti-Stokes shifted Raman photon. The aS process depends on the previous existence of the phonon in the lattice. In the case of graphene,  $E_G = 0.2$  eV is much higher than the thermal (room temperature) energy. The last diagram in Figure 5, which we call here the Stokes-anti-Stokes (SaS) event, describes a nonlinear process where a phonon created by the Stokes process is subsequently annihilated in the anti-Stokes process. The Stokes and anti-Stokes photons emerging from the SaS event can be correlated and, as discussed by Klyshko, 21 the character of this correlation can be continuously varied from purely quantum to purely classical. In order to observe the SaS scattering, we need to efficiently consume photogenerated phonons in the anti-Stokes process. Otherwise, the phonons will decohere via scattering. We also need high energy optical phonons that are unlikely to be populated at room temperature. These constrains are achieved in our  $\theta$ -defined tBLG system.

To differentiate the anti-Stokes signal originated from the SaS event from that produced by the usual aS process, we analyze the excitation laser power  $(P_{\text{laser}})$  dependence of the

anti-Stokes Raman intensity ( $I_{aS}$ ). Considering both the aS and SaS events in Figure 5 separately,  $I_{aS}$  assumes the form

$$I_{aS} = P_{laser} \{ C_{aS} \eta + C_{SaS} P_{laser} \}$$
 (1)

where  $C_{\rm aS}$  and  $C_{\rm SaS}$  are constants and  $\eta=1/[{\rm e}^{(\hbar\omega_{\rm phonon}/k_{\rm B}T)}-1]$  is the temperature dependent Bose–Einstein phonon distribution function. Here we considered  $\eta+1\approx\eta$ . The sources for  $I_{\rm aS}$  are the laser and the phonon, and the two components on the right side of eq 1 are direct consequences of the aS and SaS Feynman diagrams shown in Figure 5, respectively. The first component (aS) in eq 1 is well-known, while the second term has been proposed here. In the thermal regime, the dependence of  $I_{\rm aS}$  on  $P_{\rm laser}$  reflects the material temperature through  $\eta$ . In the regime where the SaS event dominates,  $I_{\rm aS}$  is proportional to  $P_{\rm laser}^2$ .

Figure 6 shows the power dependence of the Stokes (a) and anti-Stokes (b) signals from the tBLG (blue) and from the AB-

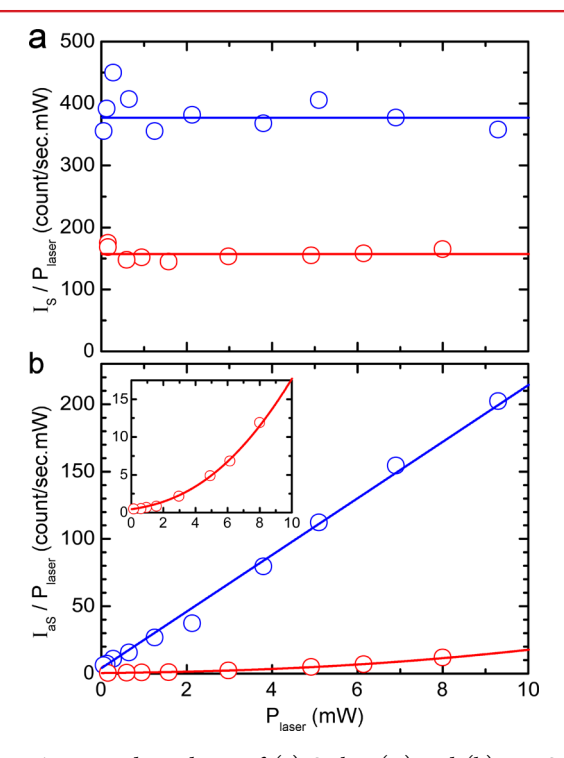


**Figure 6.** Power dependence of (a) Stokes  $(I_{\rm S})$  and (b) anti-Stokes  $(I_{\rm aS})$  Raman intensities for the tBLG (blue) and AB-BLG (red) obtained with  $E_{\rm laser}=1.96$  eV. The G band peaks were fit with a Lorentzian function. The Raman intensities were obtained from the peak integrated areas and then normalized by the laser power  $(I_{\rm S}/P_{\rm laser})$  and  $I_{\rm aS}/P_{\rm laser})$  to clearly demonstrate the difference in behavior. Circles are experimental data and lines are fitting functions according to eq 1 (see text for fitting values). The inset in (b) is a magnified version of the AB-BLG data.

BLG (red), when excited with  $E_{\rm laser}=1.96$  eV. The intensities are normalized by the excitation laser power. Figure 6a shows that the Stokes signal scales linearly with excitation power for both samples, which is indicative for the spontaneous scattering regime. However, the anti-Stokes Raman signals of the two samples show markedly different behaviors (Figure 6b).

The anti-Stokes intensity of the tBLG excited at  $E_{\rm laser}=1.96$  eV shows a quadratic power dependence within the measured range (0–10 mW, blue data in Figure 6b). The data can be accurately fitted by eq 1 considering  $\eta$  constant at T=295 K with  $C_{\rm aS}=9.1$  W<sup>-1</sup> s<sup>-1</sup> and  $C_{\rm SaS}=2.3\times10^{-9}$  W<sup>-2</sup> s<sup>-1</sup>. For

comparison, the power-normalized anti-Stokes intensity  $(I_{\rm aS}/P_{\rm laser})$  from the AB-BLG reference shows a much less pronounced enhancement within the measured range (see red data in Figure 6b) with a clear nonlinear power dependence behavior (see inset). The AB-BLG  $I_{\rm aS}/P_{\rm laser}$  data can be fit by eq 1 with  $C_{\rm aS}=1.0~{\rm W}^{-1}~{\rm s}^{-1}$ , assuming that the temperature depends linearly on the excitation laser power as  $T=295+C_{\rm T}P_{\rm laser}$  with  $C_{\rm T}=27~{\rm mW}^{-1}$  K and  $C_{\rm SaS}=0$ . According with this latest equation, for  $P_{\rm laser}>10~{\rm mW}$  the AB-BLG temperature crosses 600 °C. The AB-BLG sample burns for laser powers above 12 mW, while the tBLG withstands higher powers, evidencing the cooling process induced by the efficient anti-Stokes resonant emission in tBLG. Consistent with this picture, Figure 7 shows that the G band frequency  $(\omega_{\rm G})$  from tBLG

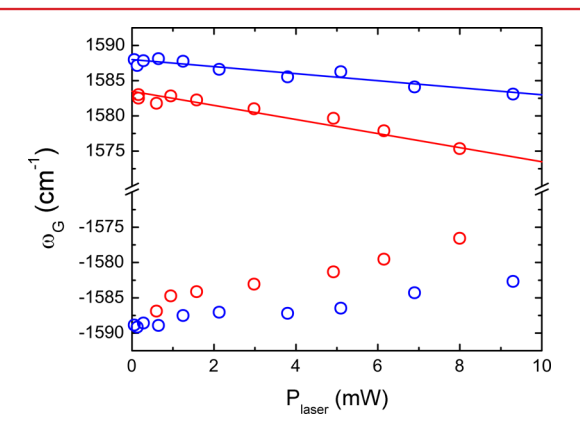


**Figure 7.** Power dependence of the G band frequencies  $\omega_{\rm G}$  for tBLG (blue) and AB-BLG (red). Positive and negative values stand for Stokes and anti-Stokes peaks, respectively. The lines are fit to the Stokes data, given by  $\omega_{\rm G}^{\rm tBLG} = 1588.0 - 0.5 P_{\rm laser}$  (blue) and  $\omega_{\rm G}^{\rm AB-BLG} = 1583.5 - 1.0 P_{\rm laser}$  (red).

(blue data) exhibits a smaller power dependence (frequency downshift with increasing power) when compared to  $\omega_{\rm G}$  from AB-BLG (red data). It is important to comment, however, that the presence of some heating in the tBLG or the SaS event in the AB-BLG reference sample cannot be ruled out from the results shown here, since a relatively small nonzero temperature increase for tBLG or  $C_{\rm SaS}$  term for AB-BLG can be added to the fitting curves without significantly compromising the fitting qualities.

The SaS process has been measured in diamond.<sup>22</sup> The experiments were carried out in the femtosecond pump regime, where the extremely high number of photons per pulse significantly enhances the SaS probability. It is surprising that our results indicate the observation of the SaS event in graphene with a significantly low power from a CW laser. Lee et al.<sup>22</sup> demonstrated the quantum nature of the SaS correlation in bulk diamond at room temperature by measuring a nonclassical SaS second-order time correlation function  $g^{(2)}$ . This type of measurement has to be developed in tBLG, so that the correlation nature of the SaS event, as proposed by Klyshko<sup>21</sup> and observed for bulk diamond,<sup>22</sup> could be explored. This effect places tBLG as a candidate for a source of entangled photons and for a host for quantum memory.<sup>21,22</sup>

It is important to make clear the reason why we built a tBLG and performed the experiment in the condition of anti-Stokes Raman resonance. When the system is in resonance with the anti-Stokes photon emission, the probability that the exciton and the phonon decay into a photon is high. Out of resonance,

the exciton and the phonon may rather decay through different processes. We actually performed similar power dependence measurements in tBLG with the 2.33 eV laser, that is, in resonance with the Stokes photon emission. The possibility that the SaS process is ruling the aS photon intensity in the Stokes resonance case cannot be ruled out. However, the signal intensities are not strong enough for the data to support this assumption (or to reject it). Therefore, the SaS process introduced may apply to graphene systems more broadly.

We expect the SaS event also to play a role in the anti-Stokes Raman scattering intensity from other low dimensional materials, like carbon nanotubes. Steiner et al.<sup>23</sup> observed laser-induced phonon cooling in single-wall carbon nanotubes by introducing them into an external optical cavity. They discussed how this scheme can be used to remove high energy hot phonons, which play an important role in the thermal and electrical properties of low-dimensional structures. 24,25 Here. we designed a system that can perform like a cooling system, but the nanostructure itself is the cavity. Because of the M-point engineering scheme used to build the tBLG, the resonance can be tuned to work at any selected wavelength from the farinfrared up to the ultraviolet, in the vibration amplifying or cooling mode, just by changing the tBLG angle  $\theta$ . Also, multiple twisted bilayer graphenes can be stacked to enhance the efficiency further (separated for example by hexagonal-BN to avoid tBLG-tBLG electronic interaction).

Finally, because Raman spectroscopy is established as an important tool to study and characterize nanostructures, our findings indicate that the SaS event has to be considered when using this technique to extract structural and transport properties of low-dimensional structures. For example, the SaS phenomena will have to be considered for quantitative analysis of temperature, thermal conductivity, and carrier dynamics, when extracted from the G band, because the peak properties (intensity, frequency, and line width) are significantly dependent on the Kohn anomaly<sup>26</sup> statistics. In future work, it will be interesting to study changes of the phonon (G band) line width and frequency as a function of detuning ( $E_{\text{opt}}$  $-E_{laser}$ ), which may change the influence of the Kohn anomaly effects in the G band properties. Furthermore, because defects change the phonon lifetimes, there could be a competition between defect scattering and the coherent anti-Stokes generation, thus opening another route for further studies.

## AUTHOR INFORMATION

## **Corresponding Author**

\*E-mail: adojorio@fisica.ufmg.br. Phone: +55 (31)34096610. Fax: +55 (31)34095600.

#### Notes

The authors declare no competing financial interest.

#### ACKNOWLEDGMENTS

The authors strongly acknowledge valuable discussions with Dr. P. Bharadwaj and L. G. Cançado. A.J. acknowledges Inmetro for the background developed in tBLG, CAPES and ETH for financing his visit to ETH Zurich. L.N. thanks financial support by the Swiss National Science Foundation (SNF) through Grant 200021-14 6358. A.V. thanks the Engineering and Physical Sciences Research Council (EPSRC) for financial support through Grants EP/G035954/1 and EP/K009451/1.

### REFERENCES

- (1) Hove, L. V. The occurrence of singularities in the elastic frequency distribution of a crystal. *Phys. Rev. B* **1953**, 89 (6), 1189.
- (2) Jorio, A.; Dresselhaus, M. S.; Saito, R. Raman Spectroscopy in Graphene Related Systems; Wiley-VCH: New York, 2011.
- (3) Mak, K. F.; Shan, J.; Heinz, T. F. Seeing many-body effects in single- and few-layer graphene: observation of two-dimensional saddle-point excitons. *Phys. Rev. Lett.* **2011**, *106*, 046401.
- (4) Mele, E. J. Commensuration and interlayer coherence in twisted bilayer graphene. *Phys. Rev. B* **2010**, *81*, R161405.
- (5) Suárez Morell, E.; Correa, J. D.; Vargas, P.; Pacheco, M.; Barticevic, Z. Flat bands in slightly twisted bilayer graphene: Tight-binding calculations. *Phys. Rev. B* **2010**, 82, R121407.
- (6) Li, G.; Luican, A.; Lopes dos Santos, J. M. B.; Castro Neto, A. H.; Reina, A.; Kong, J.; Andrei, E. Y. Observation of Von Hove singularities in twisted graphene layers. *Nat. Phys.* **2010**, *6*, 109.
- (7) Jorio, A.; Cançado, L. G. Raman spectroscopy of twisted bilayer graphene. *Solid State Commun.* **2013**, 175–176, 3.
- (8) Ni, Z.; et al. G-band Raman double resonance in twisted bilayer graphene: Evidence of band splitting and folding. *Phys. Rev. B* **2009**, 80, 125404.
- (9) Gupta, A. K.; Tang, Y.; Crespi, V. H.; Eklund, P. C. Nondispersive Raman D band activated by well-ordered interlayer interactions in rotationally stacked bilayer graphene. *Phys. Rev. B* **2010**, 82, 241406.
- (10) Carozo, V.; et al. Raman Signature of Graphene Superlattices. *Nano Lett.* **2011**, *11*, 4527.
- (11) Righi, A.; et al. Graphene Moiré patterns observed by umklapp double-resonance Raman scattering. *Phys. Rev. B* **2011**, *84*, 241409.
- (12) Havener, R. W.; Zhuang, H.; Brown, L.; Hennig, R. G.; Park, J. Angle-Resolved Raman Imaging of Interlayer Rotations and Interactions in Twisted Bilayer Graphene. *Nano Lett.* **2012**, *12*, 3162.
- (13) Kim, K.; et al. Raman spectroscopy study of rotated double-layer graphene: misorientation-angle dependence of electronic structure. *Phys. Rev. Lett.* **2012**, *108*, 246103.
- (14) Sato, K.; Saito, R.; Cong, C.; Yu, T.; Dresselhaus, M. S. Zone folding effect in Raman G-band intensity of twisted bilayer graphene. *Phys. Rev. B* **2012**, *86*, 125414.
- (15) Campos-Delgado, J.; Cançado, L. G.; Achete, C. A.; Jorio, A.; Raskin, J.-P. Raman scattering study of the phonon dispersion in twisted bilayer graphene. *Nano Res.* **2013**, *6*, 269.
- (16) Carozo, V.; et al. Resonance effects on the Raman spectra of graphene superlattices. *Phys. Rev. B* **2013**, *88*, 085401.
- (17) Havener, R. W.; Liang, Y.; Brown, L.; Yang, L.; Park, J. Van Hove Singularities and Excitonic Eects in the Optical Conductivity of Twisted Bilayer Graphene. *Nano Lett.* **2014**, *14*, 3353.
- (18) Cançado, L. G.; Jorio, A.; Pimenta, M. A. Measuring the absolute Raman cross section of nanographites as a function of laser energy and crystallite size. *Phys. Rev. B* **2007**, *76*, 064304.
- (19) Souza Filho, A. G.; Jorio, A.; Hafner, J. H.; Lieber, C. M.; Saito, R.; Pimenta, M. A.; Dresselhaus, G.; Dresselhaus, M. S. Electronic transition energy  $E_{ii}$  for an isolated (n, m) single-wall carbon nanotube obtained by anti-Stokes/Stokes resonant Raman intensity ratio. *Phys. Rev. B* **2001**, 63, 241404(R).
- (20) Jorio, A.; Souza Filho, A. G.; Dresselhaus, G.; Dresselhaus, M. S.; Saito, R.; Hafner, J. H.; Lieber, C. M.; Matinaga, F. M.; Dantas, M. S. S.; Pimenta, M. A. Joint density of electronic states for one isolated single-wall carbon nanotube studied by resonant Raman scattering. *Phys. Rev. B* **2001**, *63*, 245416.
- (21) Klyshko, D. N. Photons and Nonlinear Optics; Gordon and Breach Science Publishers: New York, 1988.
- (22) Lee, K. C.; et al. Macroscopic non-classical states and terahertz quantum processing in room-temperature diamond. *Nat. Photonics* **2012**, *6*, 41.
- (23) Steiner, M.; Qian, H.; Hartschuh, A.; Meixner, A. J. Controlling Nonequilibrium Phonon Populations in Single-Walled Carbon Nanotubes. *Nano Lett.* **2007**, *7* (8), 2239.

(24) Steiner, M.; et al. Phonon populations and electrical power dissipation in carbon nanotube transistors. *Nat. Nanotechnol.* **2009**, *4*, 320.

- (25) Barreiro, A.; Lazzeri, M.; Moser, J.; Mauri, F.; Bachtold, A. Transport properties of graphene in the high-current limit. *Phys. Rev. Lett.* **2009**, *103*, 076601.
- (26) Piscanec, S.; Lazzeri, M.; Mauri, F.; Ferrari, A. C.; Robertson, J. Kohn Anomalies and Electron-Phonon Interactions in Graphite. *Phys. Rev. Lett.* **2004**, *93*, 185503.